# Supplementary materials

## Synergistic of heterovalent valence states and oxygen vacancy defects engineering in Co/S co-doped $TiO_2$ for nitrogen photocatalytic to ammonia

Longyan Chen[1], Pengkun Zhang[1], Dong-Hau Kuo[2,*], Jianmei Jiang[1], Binghong Wu[1], Zhengjie Su[1], Osman Ahmed Zelekew[3], Jinguo Lin[1,*], Xiaoyun Chen[1,*], Dongfang Lu[1,*]

[1] College of Materials Engineering, Fujian Agriculture and Forestry University, Fuzhou 350002, China

[2] Department of Materials Science and Engineering & Graduate Institute of Energy and Sustainability Technology, National Taiwan University of Science and Technology, Taipei 10607, Taiwan

[3] Department of Materials Science and Engineering, Adama Science and Technology University, Adama, Ethiopia

*Corresponding author

*E-mail address*: dhkuo@mail.ntust.edu.tw (D. H. Kuo)

*E-mail address*: fjldf@126.com (D. Lu)

*E-mail address*: fjlinjg@126.com (J. Lin)

*E-mail address*: fjchenxy@126.com (X. Chen)

## Experimental section

### *1. Methods for determination of ammonia yield*

#### 1.1 Quantification of produced $NH_3$ using indophenol blue method.

Regarding the known literature reports [1], the reaction was carried out by mixing 4 mL of reaction solution with 50 μL of catalyst solution (aqueous solution of 1% CoTiOS), 500 μL of color developing solution (aqueous solution of 0.4 M $C_7H_5O_3Na$ and 0.32 M NaOH) and 50 μL of oxidizing solution [NaClO (ρCl = 4 – 4.9) containing 0.75 M NaOH solution] were mixed. The mixture was then allowed to stand for 2 h under ambient conditions. A standard curve was obtained from the absorbance at 660 nm. The standard curve demonstrated a strong linear relationship ($y = 0.6282x + 0.0077$, $R^2 = 0.999$). The amount of produced $NH_3$ was calculated by the correction curve obtained.

#### 1.2 Quantification of ammonia using the Ion chromatography method.

As previously reported in the literature [2], ammonia concentration analysis was performed on an ICS-3000 ion chromatography system (Dionex, Sunnyvale, CA, USA) with an analytical column (Dionex IonPac CS17, 4 × 250 mm), protective column (Dionex IonPac CG17, 4 × 50 mm), and chemical suppressor (CSRS-300, 4 mm) were used to control the flow rate of the samples at 1.0 mL/min. The leachate is a 20 mM methyl sulfonic acid aqueous solution. The conductivity cell was set at T = 35 $^{o}$C, and the injection loop volume was 25 μL. The samples were injected into the instrument for analysis using a membrane-based syringe of 0.45 μm, and the injection was repeated nine times.

### 1.3 Determination of hydrazine via Watt-Chrisp method

Configuration of hydrazine working solution: Accurately measure 0.41 g of hydrazine sulfate and dissolve it in 500 mL of secondary reagent water with 74 mL of concentrated hydrochloric acid, then transfer it to a 1 L volumetric flask. And dilute to scale with secondary reagent water. Take an appropriate amount of the reserve solution and dilute it one hundred times with hydrochloric acid solution (1: 99).

P-Dimethylaminoanisole - Sulfuric acid solution: Measure 100 mL of concentrated sulfuric acid under constant stirring and slowly add it into a beaker containing 300 mL of secondary reagent water, then add 15 g of p-Dimethylaminoanisole after cooling. After complete dissolution, it was transferred into a 500 mL brown volumetric flask, and the secondary reagent water was diluted to the scale.

Take a set of hydrazine working solution to add 5 mL p-dimethylaminoanisole-sulfuric acid solution, and let it stand for 30 min to develop the color. After 30 min, the UV-visible spectra of the sample solution corresponding to the chromogenic agent were recorded at 455 nm, and the concentration of $N_2H_4$ was estimated according to the standard calibration curves generated by the different concentrations of $N_2H_4$ (0, 0.25, 1, 2, 4, 5 mg/L).

### 1.4 Determination of nitrate ($NO_3^-$)

Quantitative analysis of $NO_3^-$ ions using UV-vis spectroscopy. For $NO_3^-$ ion detection, prepare standard stock solutions with different concentrations of $NaNO_3$, ranging from 0 to 10 $\mu mol \cdot L^{-1}$. Then take 1 mL of the standard solution and perform UV-vis measurements within the range of 200-300 nm to obtain a similar calibration curve. Similarly, the amount of $NO_3^-$ in the reaction mixture

was measured using a UV-vis spectrophotometer, where the peak at 220 nm wavelength corresponds to the absorption of nitrate, and the corresponding amount is quantified relative to the measured absorbance value.

### 1.5 Determination of $H_2O_2$

According to literature reports [3, 4], the POD-DPD method was used to determine the concentration of $H_2O_2$ in the reactants. Usually, 0.3 mL of phosphate buffer (0.5 M $K_2HPO_4$ and 0.5 M $KH_2PO_4$), 30 μL of DPD solution, and 30 μL of peroxidase were mixed with the collected solution. Then, the mixture was shaken well for 30 s and detected by UV-vis spectrophotometry at 551 nm.

## 2. Apparent quantum efficiency (AQE) and solar-to-ammonia (STA) conversion efficiency test methods

The apparent quantum efficiency (AQE) indicates the rate at which a photocatalyst utilizes incident photons at a specific monochromatic wavelength. AQE was determined under the same nitrogen fixation conditions. 50 mg CoTiOS-3 catalyst was mixed with 100 mL of deionized water without any sacrificial agent. A 300 W xenon lamp irradiated the system, and the AQE was obtained under a 420 nm filter. The AQE formula for ammonia yield [5, 6] was calculated as follows:

$$AQE = \frac{Number\ of\ reacted\ electrons}{Number\ of\ incident\ photons} = \frac{Number\ of\ generated\ NH_3 \times 6}{Number\ of\ incident\ photons} = \frac{M \times N_a \times 6}{\frac{I \times A \times \lambda \times t}{hc}}$$

here, M is the amount of produced $NH_3$, *Na* is Avogadro's constant, I is the light intensity, A is the light incident area, t is the light irradiation time, h is Plank's constant, and c is the speed of light.

According to the literature [7], to determine the STA efficiency, the reaction was carried out using an AM1.5G solar simulator, where the conversion efficiency was calculated as

$$STA = \frac{[\Delta G\ for\ NH_3\ formation\ (J/mol)] \times [NH_3\ formation\ (mol)]}{[total\ input\ energy\ (W)] \times [reaction\ time(s)]}$$

The free energy of $NH_3$ production is 339 kJ·mol$^{-1}$. The energy intensity of the AM1.5G solar irradiation (1000 W·m$^{-2}$) and the irradiated area is $4.26 \times 10^{-4}$ m$^2$. Therefore, the total input energy is 0.426 W.

## Additional tables and figures

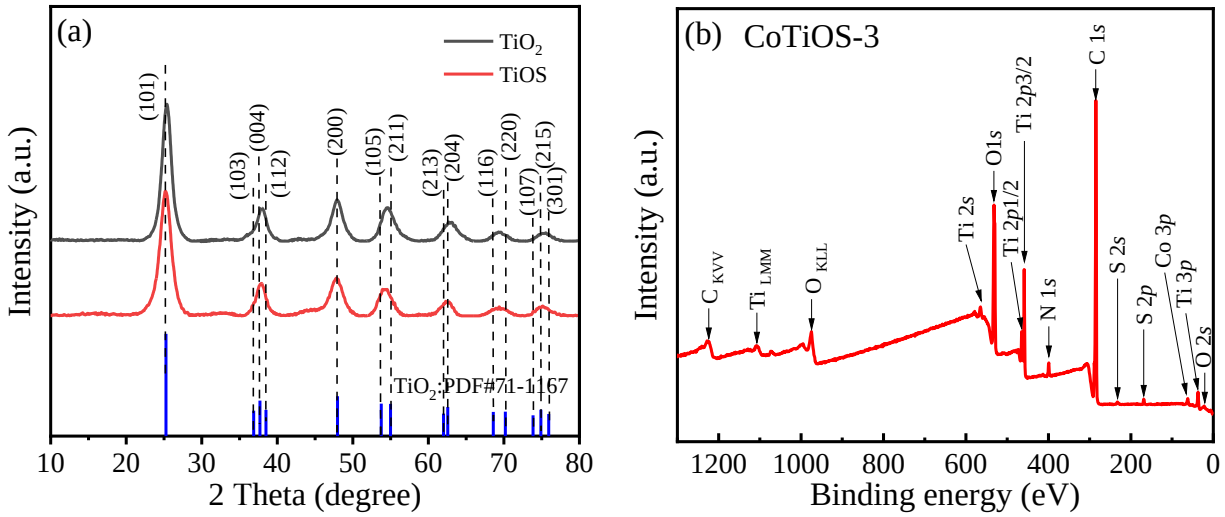


Fig. S1 (a) XRD patterns of TiOS and $TiO_2$ and standard spectrum of $TiO_2$ (#71-1167). (b) Fully scanned spectrum, XPS characterization of CoTiOS nanomaterials.

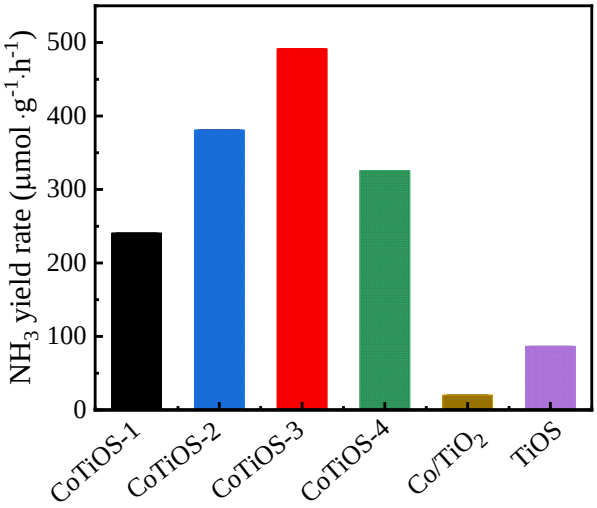


Fig. S2 Photocatalytic $N_2$ fixation activity test of different samples.

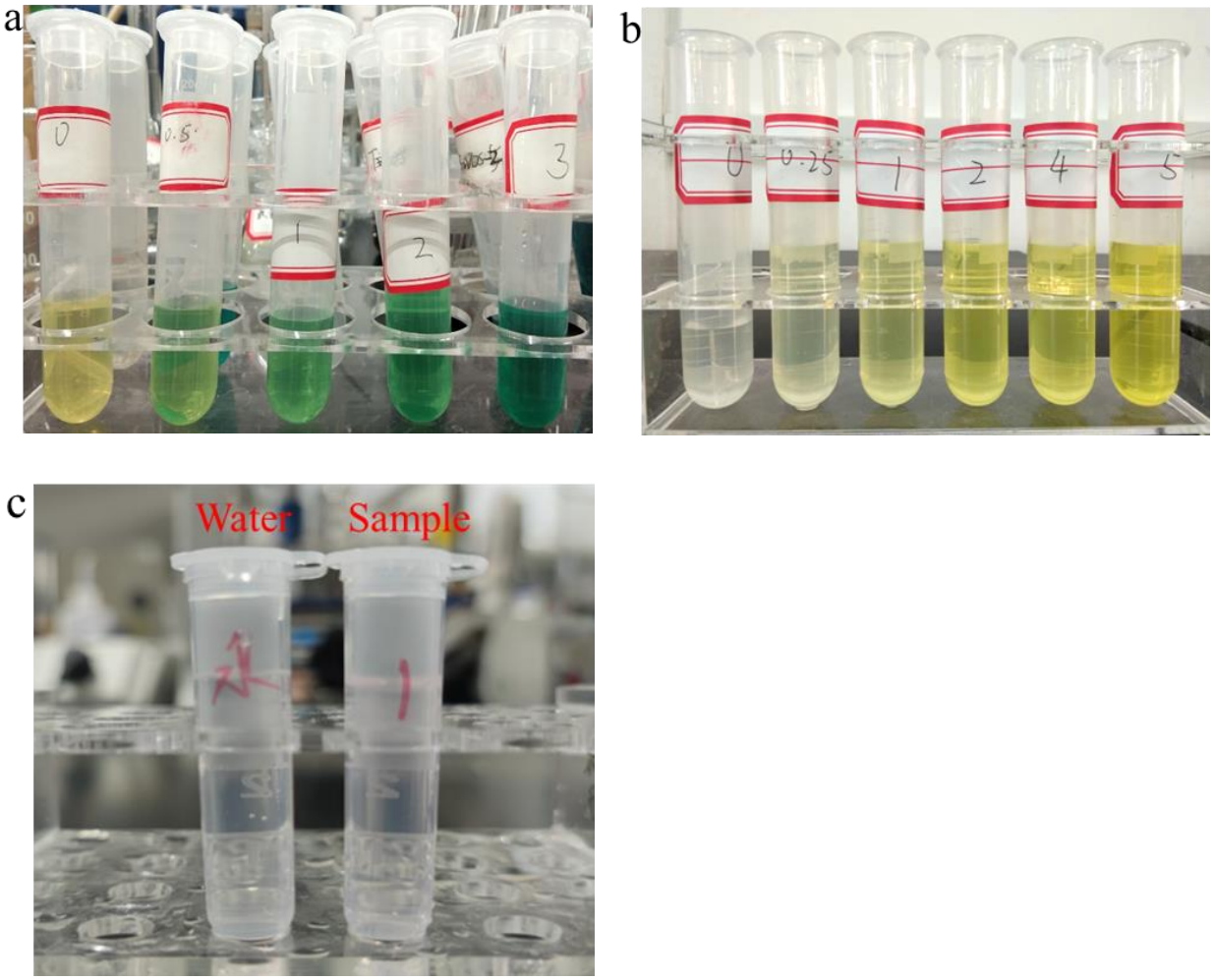


Fig. S3 (a) The picture for chromogenic reaction graphs of the indophenol blue reagent method in photocatalytic $N_2$ stationary system with 0, 0.5, 1, 2, and 3 mL of standard solution (from left to right), respectively. (b) Color reaction diagrams of $N_2H_4$ at 0, 0.25, 1, 2, 4, and 5 mL. (c) The color change of the mixed solution when measuring $H_2O_2$.

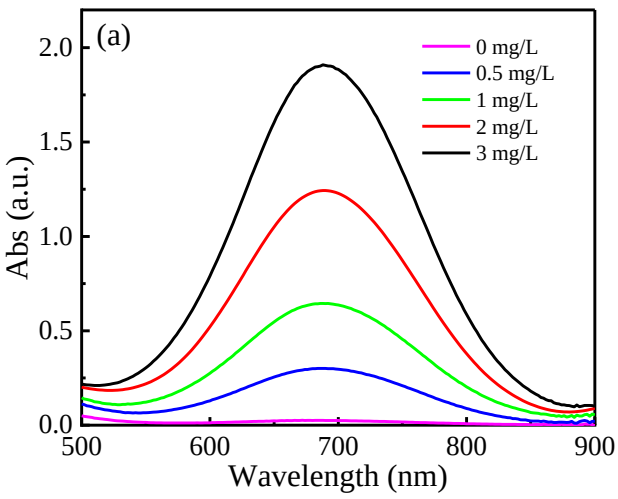


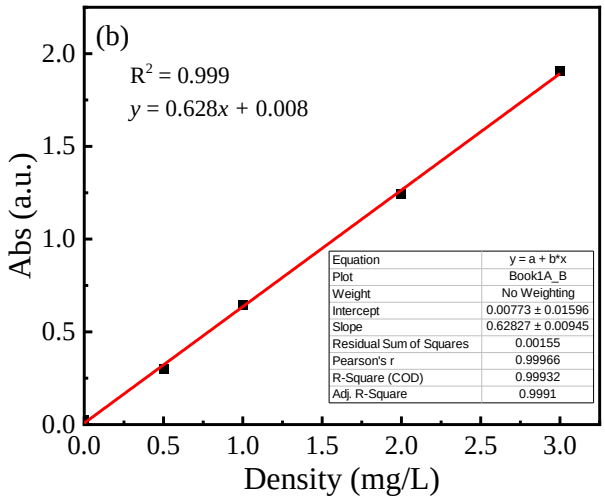


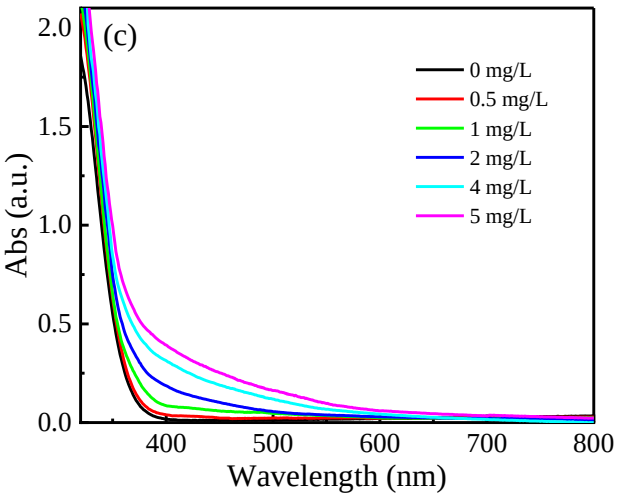


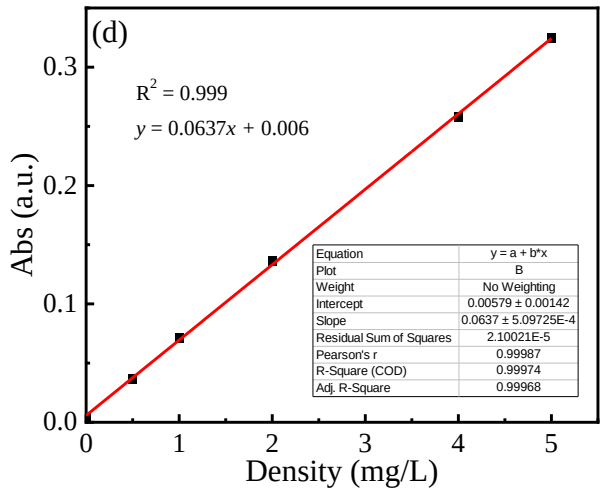


(e)

| Injection Name | Ret.Time min ECD_1 | Area µS*min ECD_1 | Height µS ECD_1 | Amount ECD_1 |
|---|---|---|---|---|
| | NH4+ | NH4+ | NH4+ | NH4+ |
| 0.5 | 4.757 | 0.0615 | 0.409 | 0.273 |
| 1 | 4.764 | 0.1184 | 0.772 | 0.920 |
| 2 | 4.767 | 0.2203 | 1.402 | 2.104 |
| 5 | 4.781 | 0.4793 | 2.851 | 5.279 |
| 10 | 4.774 | 0.8392 | 4.753 | 10.197 |
| 20 | 4.787 | 1.3800 | 7.448 | 19.439 |
| 30 | 4.787 | 1.7911 | 9.359 | 30.373 |
| 40 | 4.797 | 2.1545 | 11.008 | n.a. |
| 50 | 4.807 | 2.5703 | 12.926 | n.a. |
| Average | 4.780 | | | |
| Rel. Std. Dev. | 0.341 % | | | |

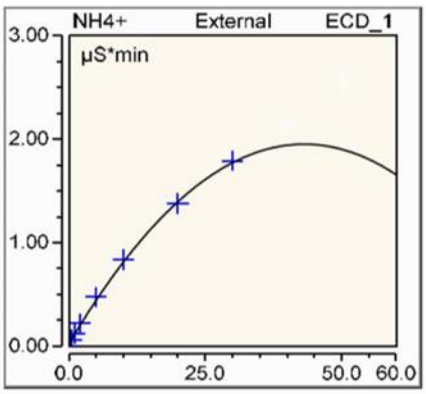

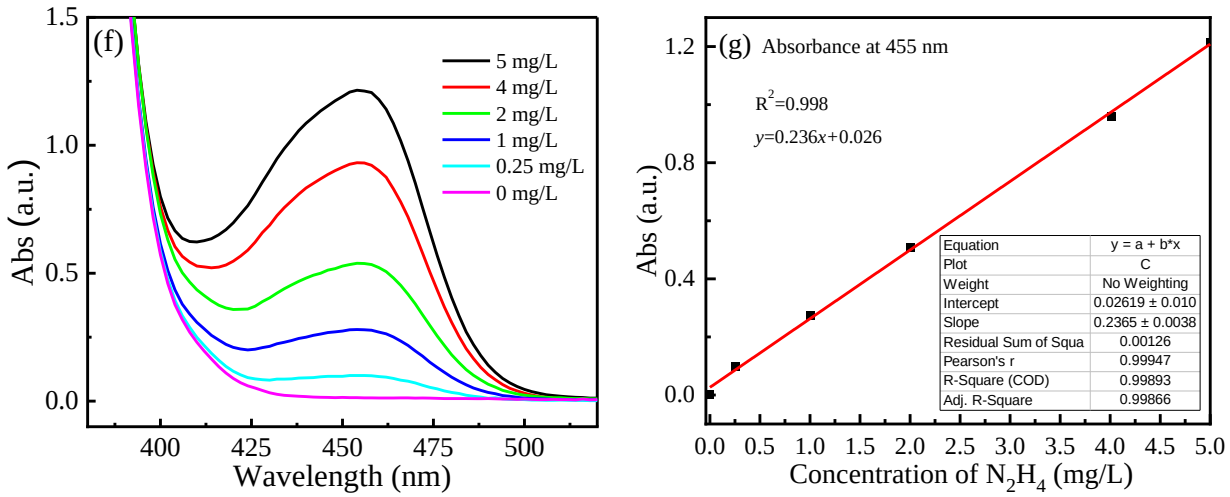


Fig. S4 (a, b) The standard curve of indophenol blue method and (c, d) Nessler's reagent, (e) The concentration of ammonium ions was detected by cation ion chromatography. $N_2H_4$ quantification method. (f) UV-vis absorption spectra and (g) corresponding calibration curves for the colorimetric $N_2H_4$ with linear fit analysis showing good linear correlation ($y = 0.236x + 0.026$, $R^2 = 0.998$).

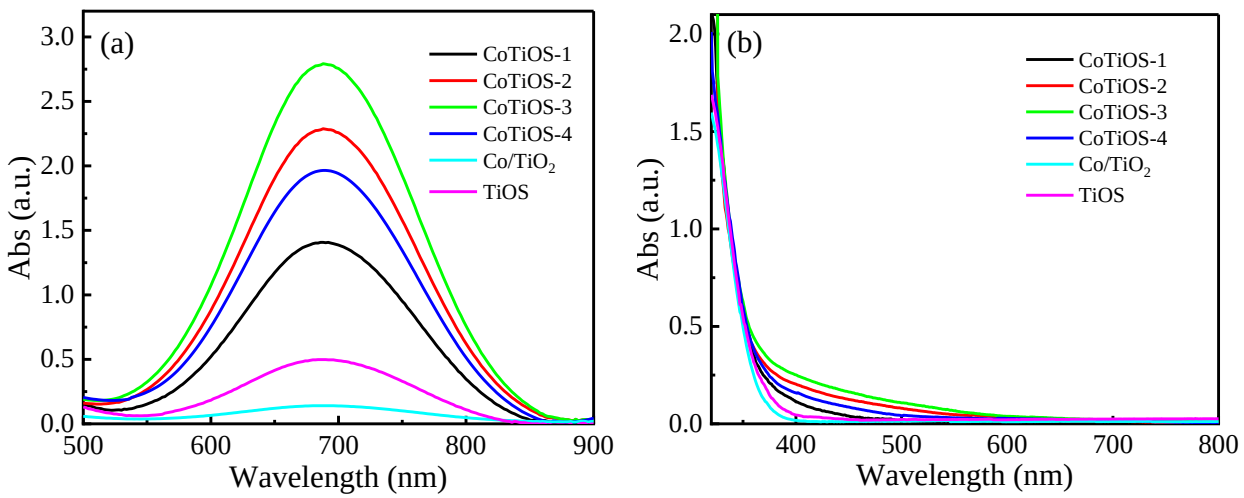


Fig. S5 The test results of (a) indophenol blue, (b) Nessler's reagent.

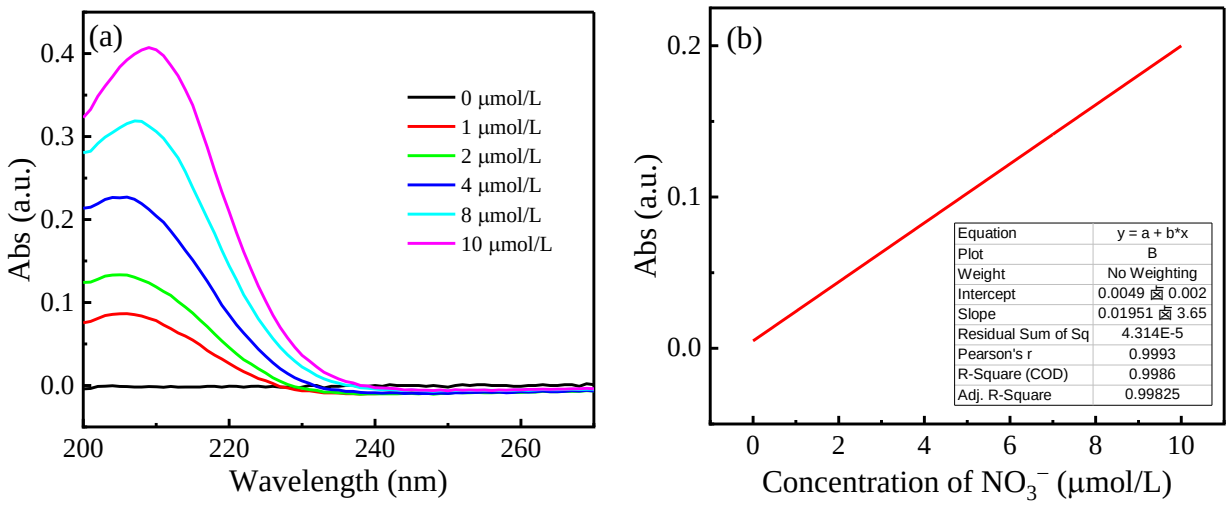


Fig. S6 Absorption spectra and calibration curve for (a, b) $NO_3^-$ ion detection.

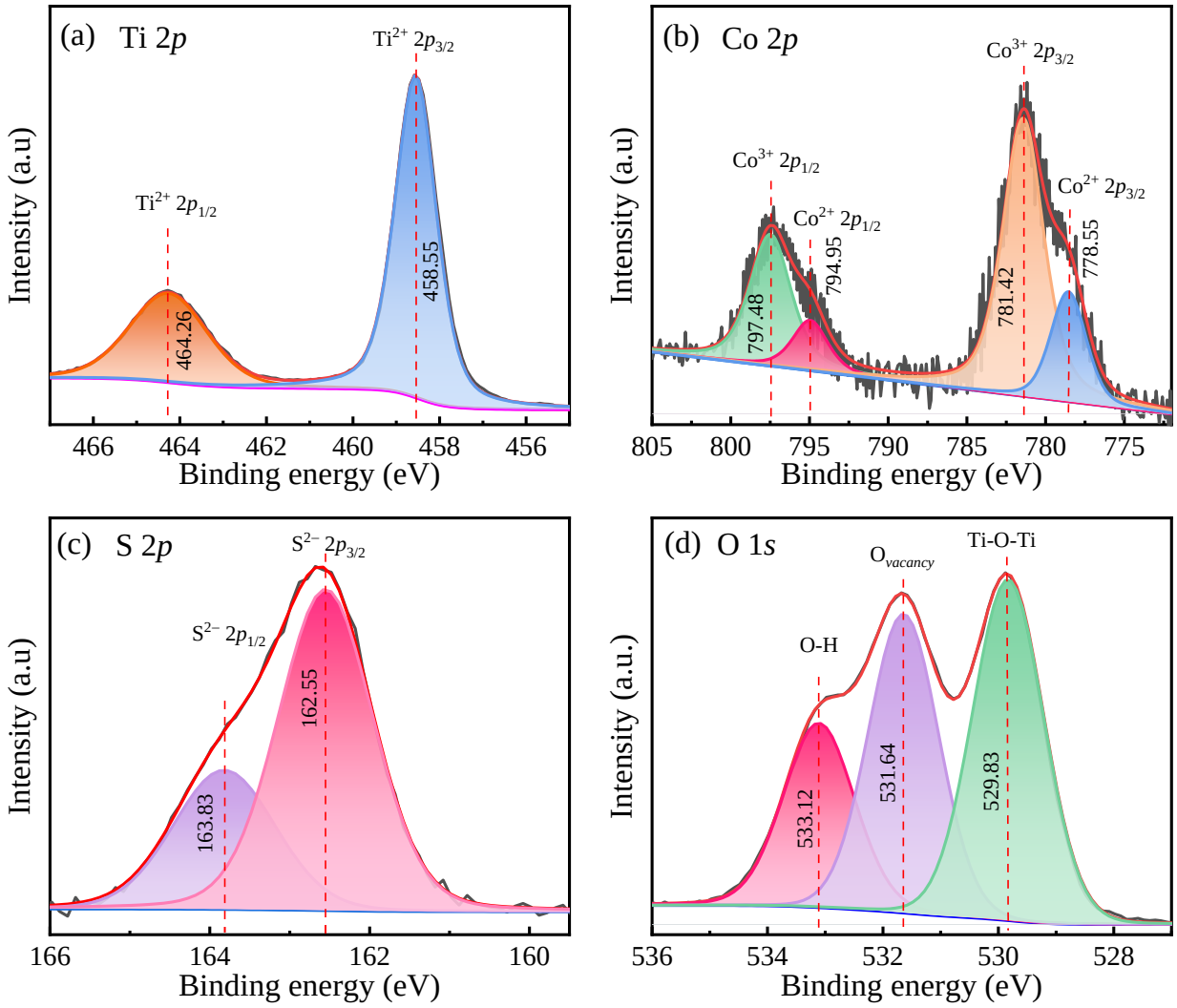


Fig. S7 High-resolution XPS tests for (a) Ti 2*p*, (b) Co 2*p*, (c) S 2*p*, and (d) O 1*s*, respectively, after the reaction.

**Table S1** XPS composition and physical characteristics of CoTiOS, Co/$TiO_2$, and TiOS catalysts.

| Sample | atomic percentage/% | | | | O molar percentage/% | | $Co^{2+}/Co^{3+}$ (%) | Crystal size (nm) | $S_{BET}$ ($m^2/g$) | Pore volume ($cm^3/g$) |
|---|---|---|---|---|---|---|---|---|---|---|
| | Co | Ti | S | O | $O_{Lattice}$ | $O_v$ | | | | |
| CoTiOS-1 | 4.39 | 26.06 | 4.15 | 65.40 | 78.54 | 21.46 | 4.02 | 4.8 | 161.9 | 0.176 |
| CoTiOS-2 | 4.44 | 25.93 | 5.69 | 63.94 | 66.42 | 33.58 | 10.65 | 4.7 | 162.1 | 0.182 |
| CoTiOS-3 | 4.66 | 26.12 | 6.73 | 62.49 | 53.66 | 46.34 | 15.42 | 4.9 | 162.6 | 0.191 |
| CoTiOS-4 | 4.57 | 26.28 | 7.65 | 61.50 | 74.93 | 25.07 | 13.85 | 4.5 | 162.3 | 0.185 |
| Co/$TiO_2$ | 4.42 | 26.15 | – | 69.43 | 100 | – | – | 4.6 | 100.8 | 0.114 |
| TiOS | – | 32.61 | 6.51 | 60.88 | 80.24 | 19.76 | – | 4.9 | 106.4 | 0.123 |
| CoTiOS-3 after reaction | 4.61 | 26.08 | 6.74 | 62.57 | 53.59 | 46.41 | 15.36 | 5.0 | – | – |

**Table S2** Elements contents from SEM-EDS analysis for samples.

| Catalyst | Co (%) | Ti (%) | S (%) | O (%) | Ti/Co (%) |
|---|---|---|---|---|---|
| CoTiOS-1 | 3.47 | 25.75 | 4.25 | 66.53 | 7.42 |
| CoTiOS-2 | 3.35 | 25.86 | 5.87 | 64.92 | 7.72 |
| CoTiOS-3 | 3.29 | 26.02 | 7.12 | 63.57 | 7.91 |
| CoTiOS-4 | 3.32 | 25.94 | 7.85 | 62.89 | 7.81 |
| Co/$TiO_2$ | 3.44 | 26.28 | – | 70.28 | 7.64 |
| TiOS | – | 31.97 | 6.54 | 61.51 | – |

**Table S3** Element analyses tested by XRF.

| Catalyst | Co (%) | Ti (%) | S (%) | O (%) | Ti/Co (%) |
|---|---|---|---|---|---|
| CoTiOS-1 | 3.99 | 26.54 | 4.01 | 65.43 | 6.65 |
| CoTiOS-2 | 4.02 | 26.56 | 5.43 | 63.99 | 6.61 |
| CoTiOS-3 | 4.10 | 26.79 | 6.75 | 62.36 | 6.53 |
| CoTiOS-4 | 4.17 | 26.85 | 7.69 | 61.29 | 6.44 |
| $Co/TiO_2$ | 4.06 | 26.86 | – | 69.18 | 6.62 |
| TiOS | – | 32.02 | 6.14 | 61.84 | – |

**Table S4** Statistics of test results of catalyst CoTiOS on Nessler's reagent, indophenol blue, and cation ion chromatography methods.

| Catalyst | Nessler's reagent ($\mu mol \cdot g^{-1} \cdot h^{-1}$) | indophenol blue ($\mu mol \cdot g^{-1} \cdot h^{-1}$) | ion chromatography ($\mu mol \cdot g^{-1} \cdot h^{-1}$) |
|---|---|---|---|
| CoTiOS-1 | 240.63 | 244.78 | 221.43 |
| CoTiOS-2 | 380.81 | 369.85 | 354.12 |
| CoTiOS-3 | 491.56 | 472.42 | 464.48 |
| CoTiOS-4 | 325.74 | 310.77 | 308.64 |
| $Co/TiO_2$ | 20.12 | 19.52 | 18.56 |
| TiOS | 86.56 | 78.46 | 73.21 |

**Table S5** Overview of reduction of $N_2$ to $NH_3$ by other photocatalysts.

| Photocatalyst | Light source | Reaction media | $NH_3$ yield rate ($\mu mol \cdot g^{-1} \cdot h^{-1}$) | AQE (%) | $N_2$ Source | Refs. |
|---|---|---|---|---|---|---|
| **FeN-CDs/$TiO_2$@CN** | 300 W Xe | 5 wt% aqueous methanol | 550.9 | – | $N_2$ | [8] |
| **Bi-$CdMoO_4$** | 300 W Xe | Methanol solution | 118 | – | $N_2$ | [9] |
| **$MoS_2$/UiO-66(SH)$_2$** | visible light $\lambda > 400$ nm | Water | 54.08 | 5.1% 400 nm | $N_2$ | [10] |
| **$TiO_{2-x}$-Ag@HKUST-1/carbon paper** | visible light $\lambda = 450$ nm | Water | 624.7 | 2.08% 450 nm | $N_2$ | [11] |
| **GO/$MoS_2$/$Ag_3PO_4$** | 300 W Xe $\lambda > 420$ nm | $Na_2SO_3$ solution | 17.5 | 0.063% 400 nm | $N_2$ | [12] |
| **$CeCO_3OH$** | Visible light | Water | 650 | 1% 300 nm | $N_2$ | [13] |
| **$BiCN_{x-5}$** | 300 W Xe $\lambda > 420$ nm | $Na_2SO_3$ solution | 576.11 | 0.53% 400 nm | $N_2$ | [14] |
| **$TiO_2$/CuO** | 400 W Hg | Water | 1.58 | – | $N_2$ | [15] |
| **$SrTiO_3$** | 300 W Xe | Water | 206.0 | 0.38% 420 nm | $N_2$ | [16] |
| **Au/$TiO_2$** | 300 W Xe $\lambda > 420$ nm | 10% methanol aqueous | 78.60 | 0.82% 550 nm | $N_2$ | [17] |
| **$Ru_1$/$TiO_2$-Vo** | 300 W Xe | Water | 18.9 | – | $N_2$ | [18] |
| **MXene/$TiO_2$** | 300 W Xe | Water | 110 | – | $N_2$ | [19] |
| **Ni-doped $TiO_2$** | 300 W Xe | Water | 46.8 | – | $N_2$ | [20] |
| **$TiO_2$ NBAs** | 300 W Xe | Water | 178 | 0.12% 405 nm | $N_2$ | [21] |
| **$TiO_2$ Vo@PNIPAm** | 400 W Hg | Water | 11.12 | – | $N_2$ | [22] |
| **1 *wt*% Ru-$TiO_2$** | 300 W Xe | 20% ethanol solution | 3.31 | – | $N_2$ | [23] |
| **Cu-doped $TiO_2$** | 300 W Xe | Water | 78.90 | 0.23% 420 nm | $N_2$ | [24] |
| **AgPt-$TiO_2$** | 300 W Xe | Water | 38.4 | – | $N_2$ | [25] |
| **CoTiOS-3** | 300 W Xe ($\lambda > 420$ nm) | Water | 491.56 | 1.89% 420 nm | $N_2$ | This work |

## References:


[1] T. Hu, G. Jiang, Y. Yan, S. Lan, J. Xie, Q. Zhang, Y. Li, Facile synthesis of Fe single-atom porous photocatalysts via direct metal atomization achieving efficient photocatalytic nitrogen fixation, *J Mater Sci Technol*. 167 (2023) 248–257.

[2] L. Rastogi, D. Ankam, S. Yadlapalli, K. Dash, Development of microwave assisted-UV digestion using diluted reagents for the determination of total nitrogen in cereals by ion chromatography, *Curr Res Food Sci*. 4 (2021) 421–428.

[3] W. Liu, C. Song, M. Kou, Y. Wang, Y. Deng, T. Shimada, L. Ye, Fabrication of ultrathin g-$C_3N_4$ nanoplates for efficient visible-light photocatalytic $H_2O_2$ production via two-electron oxygen reduction, *Chem. Eng. J.* 425 (2021) 130615.

[4] H. Luo, T. Shan, J. Zhou, L. Huang, L. Chen, R. Sa, Y. Yamauchi, J. You, Y. Asakura, Z. Yuan, H. Xiao, Controlled synthesis of hollow carbon ring incorporated g-$C_3N_4$ tubes for boosting photocatalytic $H_2O_2$ production, *Appl Catal B-Environ.* 337 (2023) 122933.

[5] C. Choong, C. Park, Y. Chang, J. Yang, J. Kim, S. Oh, B. Jeon, E. Choi, Y. Yoon, M. Jang, Interfacial coupling perovskite $CeFeO_3$ on layered graphitic carbon nitride as a multifunctional Z-scheme photocatalyst for boosting nitrogen fixation and organic pollutants demineralization, *Chem. Eng. J*. 427 (2022) 131406.

[6] H. Luo, J. Yan, Y. Shan, J. Zhou, J. Yu, B. Boury, H. Wu, H. Xiao, L. Huang, Z. Yuan, L. Chen, Metal-free photocatalyst for nitrogen fixation under visible light based on COF/g-$C_3N_4$/CNT nanocomposite, *J. Environ. Chem. Eng*. 10 (2022) 107713.

[7] X. Yu, P. Qiu, Y. Wang, B. He, X. Xu, H. Zhu, J. Ding, X. Liu, Z. Li, Y. Wang, Defect-induced charge redistribution of $MoO_{3-x}$ nanometric wires for photocatalytic ammonia synthesis, *J.*

*Colloid Interface Sci.* 640 (2023) 775−782.

[8] K. Li, C. Sun, Z. Chen, H. Qu, H. Xie, Q. Zhong, Fe-carbon dots enhance the photocatalytic nitrogen fixation activity of $TiO_2$@CN heterojunction, *Chem. Eng. J.* 429 (2022) 132440.

[9] J. Wang, L. Guan, S. Yuan, J. Zhang, C. Zhao, X. Hu, B. Teng, Y. Wu, Y. He, Greatly boosted photocatalytic $N_2$-to-$NH_3$ conversion by bismuth doping in $CdMoO_4$: Band structure engineering and $N_2$ adsorption modification, *Sep. Purif. Technol.* 314 (2023) 123554.

[10] Q. Li, Y. Shi, Z. Wang, C. Liu, J. Bi, J. C. Yu, L. Wu, Nitrogen activation and surface charge regulation for enhancing the visible-light-driven $N_2$ fixation over $MoS_2$/UiO-66$(SH)_2$, *J. Colloid Interface Sci.* 652 (2023) 1568−1577.

[11] H. Zhao, J. Duan, Z. Zhang, W. Wang, High-performance gas-liquid-solid optofluidic microreactor with $TiO_{2-x}$-Ag@HKUST-1/carbon paper for efficient photocatalytic nitrogen fixation to ammonia, *Colloid Surface A*. 660 (2023) 130874.

[12] K. Zhao, Y. Feng, Z. Zhang, H. Li, X. Gao, S. Lin, Enhanced spatial charge separation at surface & interface via GO/$MoS_2$/$Ag_3PO_4$ ternary Z-scheme heterostructure for nitrogen photo-fixation, *Appl Catal A-Gen*. 646 (2022) 118850.

[13] H. Zhang, Y. Chen, L. Bao, Y.-J. Yuan, Double quantum dots decorated layer structure $CeCO_3OH$ for improved $N_2$ photo-fixation, *J Catal*. 412 (2022) 1–9.

[14] C. Liang, H. Niu, H. Guo, C. Niu, Y. Yang, H. Liu, W. Tang, H. Feng, Efficient photocatalytic nitrogen fixation to ammonia over bismuth monoxide quantum dots-modified defective ultrathin graphitic carbon nitride, *Chem. Eng. J.* 406 (2021) 126868.

[15] H. Lee, J. Lee, Y. Lee, E. Cho, Y. Jang, Boosting solar-driven $N_2$ to $NH_3$ conversion using defect-engineered $TiO_2$/CuO heterojunction photocatalyst, *Appl. Surf. Sci.* 620 (2023) 156812.

[16] J. Wang, T. Wang, Z. Zhao, R. Wang, C. Wang, F. Zhou, S. Li, L. Zhao, M. Feng, Regulation of oxygen vacancies in $SrTiO_3$ perovskite for efficient photocatalytic nitrogen fixation, *Journal of Alloys and Compounds: An Interdisciplinary Journal of Materials Science and Solid-state Chemistry and Physics*, 902 (2022) 163865–163872.

[17] J. Yang, Y. Guo, R. Jiang, F. Qin, H. Zhang, W. Lu, J. Wang, J.C. Yu, High-efficiency "working-in-tandem" nitrogen photofixation achieved by assembling plasmonic gold nanocrystals on ultrathin titania nanosheets, *J. Am. Chem. Soc.,* 140 (2018) 8497.

[18] G. Ren, M. Shi, S. Liu, Z. Li, Z. Zhang, X. Meng, Molecular-level insight into photocatalytic reduction of $N_2$ over Ruthenium single atom modified $TiO_2$ by electronic metal-support interaction, *Chem. Eng. J*. 454 (2023) 140158.

[19] W. Gao, X. Li, S. Luo, Z. Luo, X. Zhang, R. Huang, M. Luo, In situ modification of cobalt on MXene/$TiO_2$ as composite photocatalyst for efficient nitrogen fixation, *J. Colloid Interface Sci.* 585 (2021) 20–29.

[20] J. Li, D. Wang, R. Guan, Y. Zhang, Z. Zhao, H. Zhai, Z. Sun, Vacancy-enabled mesoporous $TiO_2$ modulated by nickel doping with enhanced photocatalytic nitrogen fixation performance, *ACS Sustain. Chem. Eng.* 8 (2020) 18258–18265.

[21] Y. Zhang, X. Chen, S. Zhang, L. Yin, Y. Yang, Defective titanium dioxide nanobamboo arrays architecture for photocatalytic nitrogen fixation up to 780 nm, *Chem. Eng. J*. 401 (2020) 126033.

[22] C. Lee, H. Kim, Y.J. Jang, Three phase boundary engineering using hydrophilic–hydrophobic poly (N-isopropylacrylamide) with oxygen-vacant $TiO_2$ photocatalysts for photocatalytic $N_2$ reduction, *ACS Appl. Energy Mater.* 5 (2022) 11018–11024.

[23] S. Liu, Y. Wang, S. Wang, M. You, S. Hong, T.-S. Wu, Y.-L. Soo, Z. Zhao, G. Jiang, J. Qiu,

Photocatalytic fixation of nitrogen to ammonia by single Ru atom decorated $TiO_2$ nanosheets, *ACS Sustain. Chem. Eng.* 7 (2019) 6813–6820.

[24] Y. Zhao, Y. Zhao, R. Shi, B. Wang, G.I.N. Waterhouse, L.Z. Wu, C.H. Tung, T. Zhang, Tuning oxygen vacancies in ultrathin $TiO_2$ nanosheets to boost photocatalytic nitrogen fixation up to 700 nm, *Adv. Mater.,* 31 (2019) 1806482.

[25] X. Bian, Y. Zhao, S. Zhang, D. Li, R. Shi, C. Zhou, L.Z. Wu, T. Zhang, Enhancing the supply of activated hydrogen to promote photocatalytic nitrogen fixation. *ACS Mater. Lett.*, 3 (2021) 1521–1527.